



# Nonuniformity in ligaments is a structural strategy for optimizing functionality

Gili R. S. Naveh<sup>a,b,1</sup>, Jonathan E. Foster<sup>a</sup>, Tomas M. Silva Santisteban<sup>c</sup>, Xianrui Yang<sup>a</sup>, and Bjorn R. Olsen<sup>a</sup>

<sup>a</sup>Department of Developmental Biology, Harvard School of Dental Medicine, Harvard University, Boston, MA 02115; <sup>b</sup>Department of Orthodontics and Craniofacial Orthopedics, School of Dental Medicine, Boston University, Boston, MA 02118; and <sup>c</sup>Materials and Structural Analysis Division, Thermo Fisher Scientific, Houston, TX 77084

Edited by Lia Addadi, Weizmann Institute of Science, Rehovot, Israel, and approved July 26, 2018 (received for review May 8, 2018)

**Ligaments serve as compliant connectors between hard tissues. In that role, they function under various load regimes and directions. The 3D structure of ligaments is considered to form as a uniform entity that changes due to function. The periodontal ligament (PDL) connects the tooth to the bone and sustains different types of loads in various directions. Using the PDL as a model, employing a fabricated motorized setup in a microCT, we demonstrate that the fibrous network structure within the PDL is not uniform, even before the tooth becomes functional. Utilizing morphological automated segmentation methods, directionality analysis, as well as second harmonic generation imaging, we find high correlation between blood vessel distribution and fiber density. We also show a structural feature in a form of a dense collar around the neck of the tooth as well as a preferred direction of the fibrous network. Finally, we show that the PDL develops as a nonuniform structure, with an architecture designed to sustain specific types of load in designated areas. Based on these findings, we propose that ligaments in general should be regarded as nonuniform entities, structured already at developmental stages for optimal functioning under variable load regimes.**

periodontal ligament | nonuniformity | fiber directionality | microCT | fiber segmentation

Skeletal locomotion is vital for function and survival. Whereas a large range of motion is desirable, restriction of this range is of no less importance. The framework of the range of motion is defined by bone morphology, but mostly by ligaments that restrain the mobility of bones across joints. As connectors between bones, ligaments also have a role in bone formation and remodeling processes. However, despite their central functional roles, the structure, regeneration, and healing abilities of ligaments are not well understood.

Ligaments are composed of collagens, glycosaminoglycans (GAGs), fibroblasts, water, and blood vessels. The collagenous component is mainly type I collagen; however, other collagen types, such as II–VI, XI, XII, and XIV, are also found in ligaments and at their bony interfaces (1–5). Type I collagen, for example, is known to have low compressive properties in hydrated state; therefore, in areas of ligaments that are working under compression loads as well as in pathological conditions, a mixture of type II collagen and GAGs which absorb compressive loads efficiently, are found (6). The distribution and composition of these components within the ligament is therefore associated with function (6–8); however, the onset and process of functional alterations of the ligament structure as well as correlation to vascular changes are yet to be demonstrated. Structure and function are intermingled and inseparable. On one hand, nonuniform distribution of different collagens, GAGs, and blood vessels is a consequence of function; on the other hand, the nonuniformity itself also affects tissue properties such as stiffness of the extracellular matrix and surface roughness—properties which are known to influence cell motility and differentiation, and therefore function. The order of events however is mostly obscure (9, 10). This study is aimed at investigating this order and testing the hypothesis that nonuniformity within ligaments

precedes, and therefore guides, function. To do so, we have studied the periodontal ligament (PDL) which connects the teeth to the maxillary and mandibular bones. Teeth do not have regeneration capabilities; nonetheless, they sustain high and repetitive loads in variable directions. Their survival is therefore essentially attributed to their ability to move and deform. Being the only soft tissue in the entire tooth–bone complex, the PDL controls tooth movement and is therefore vital for tooth survival. Similar to other ligaments, the PDL consists of collagens, glycosaminoglycans, fibroblasts, water, and blood vessels. The major collagenous constituent is type I, and it is the only collagen that is embedded in both the tooth and the bone. Other types of collagen in the PDL are types III, V, VI, and XII (11, 12). It was previously shown that the 3D collagenous network in rat PDL is not uniform in its distribution (13). In this study, using a mouse model, we investigate whether the nonuniformity is a developmental feature that precedes and therefore guides function or whether the nonuniformity is a result of function. Using a humidified custom-made chamber, coupled with a loading system, we generated 3D imaging at high resolution of the collagen fibers in fresh specimens without fixation or staining and correlated the structure with tooth function. An in-house automated segmentation algorithm allowed us to objectively trace and segment the PDL fibrous components and generate 3D distribution maps and directionality analysis of the fibrous components at different functional stages.

## Results

A customized loading system inside the microCT (Xradia micro XCT-200, Zeiss) (detailed description in *SI Appendix*) provides

### Significance

**Structure and function are intermingled and inseparable. Therefore, the structure–function dependency sequence is mostly unclear. Using the periodontal ligament as a model, employing a technique utilizing a loading system inside a microCT, we were able to visualize in 3D the fresh collagen networks and correlate their distribution and direction with loads exerted on the ligament. We show that the ligament structure is not uniform and is determined before it becomes functional, and therefore we propose that structural nonuniformity is specifically designed to optimize ligament function to the variable forces it sustains.**

Author contributions: G.R.S.N. and B.R.O. designed research; G.R.S.N. and X.Y. performed research; G.R.S.N. and T.M.S.S. contributed new reagents/analytic tools; G.R.S.N. and J.E.F. analyzed data; and G.R.S.N., J.E.F., and B.R.O. wrote the paper.

The authors declare no conflict of interest.

This article is a PNAS Direct Submission.

This open access article is distributed under [Creative Commons Attribution-NonCommercial-NoDerivatives License 4.0 \(CC BY-NC-ND\)](https://creativecommons.org/licenses/by-nc-nd/4.0/).

<sup>1</sup>To whom correspondence should be addressed. Email: gili\_naveh@hdsdm.harvard.edu.

This article contains supporting information online at [www.pnas.org/lookup/suppl/doi:10.1073/pnas.1807324115/-DCSupplemental](http://www.pnas.org/lookup/suppl/doi:10.1073/pnas.1807324115/-DCSupplemental).

Published online August 20, 2018.

phase enhancement which enables 3D visualization of the fibrous network of a fresh and intact PDL due to humidified conditions and mechanical stabilization (13, 14). Using a mouse molar tooth we were able to reach a high resolution with a voxel size of  $0.79\ \mu\text{m}$  and generate a detailed structural analysis of the collagen networks inside the PDL.

**A 3D Visualization of the PDL Collagen Networks.** The 3D images of fresh and unsectioned PDL reveal that the fibrous network is organized in longitudinal sheets along the long axis of the roots and not in bundles as described in the literature (Fig. 1*A*). To analyze the different structural features of the collagen networks, we segmented out the tooth and the bone computationally based on morphological features rather than gray values (detailed information about the process can be found in *SI Appendix*). The segmented PDL images show the longitudinal backbone organization of fibers; however, oblique and horizontal components exist between the longitudinal scaffolds. Together, the longitudinal scaffold and horizontal components are distributed non-uniformly throughout the PDL. There are areas of high fiber concentrations—dense networks (Fig. 1, black arrowheads) while other areas have very few fibers—sparse networks (Fig. 1, gray arrowheads). The sparse networks are seen in the area between the roots—the furcation area (Fig. 1*C*)—and in the middle of the roots on the buccal side (Fig. 1*E*).

**Characterizing the Collagen Distribution.** Fiber density maps (Fig. 2) were generated to objectively evaluate the locations of dense and sparse networks (the algorithm is described in *SI Appendix*). The density maps show a distinct difference between fiber organization at the buccal and lingual sides of the root. In general the lingual side presents a uniform dense network (Fig. 2*B*), whereas the buccal side contains a dense network strip close to the crown of the tooth (black arrows); however, the middle area

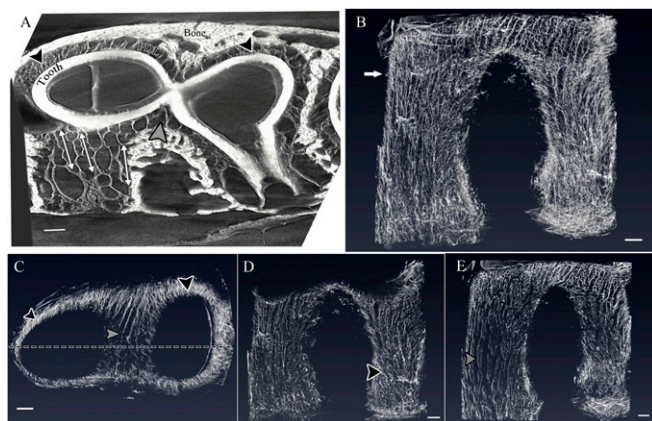


**Fig. 1.** The 3D visualization of fresh, unstained collagen networks in the periodontal ligament of a 15-wk-old mouse's first mandibular molar. Gray arrowheads show sparse networks; black arrowheads, dense networks. (Scale bars:  $100\ \mu\text{m}$ .) (*A*) Reconstructed volume showing the first molar tooth of a mouse inside the bone and the collagenous component of the PDL. Two directional arrows show the longitudinal orientation of the collagen sheets; bone is virtually removed. (*B*) A 3D view of only the collagen network of the PDL, in a sagittal orientation. (*C*) Transverse view of the upper portion of the collagen network, the portion above the white arrow in *B*, showing the sparse network in between the roots, the furcation (gray arrowhead), and the dense areas encircling the roots (black arrowheads). (*D*) Sagittal section (made at the dashed line *C*) showing the collagen network on the tongue side of the tooth (below dashed line); black arrowhead points to the most noticeable dense area. (*E*) Sagittal section showing the collagen network on the cheek side of the tooth (above dashed line); gray arrowhead points to the most noticeable sparse area.

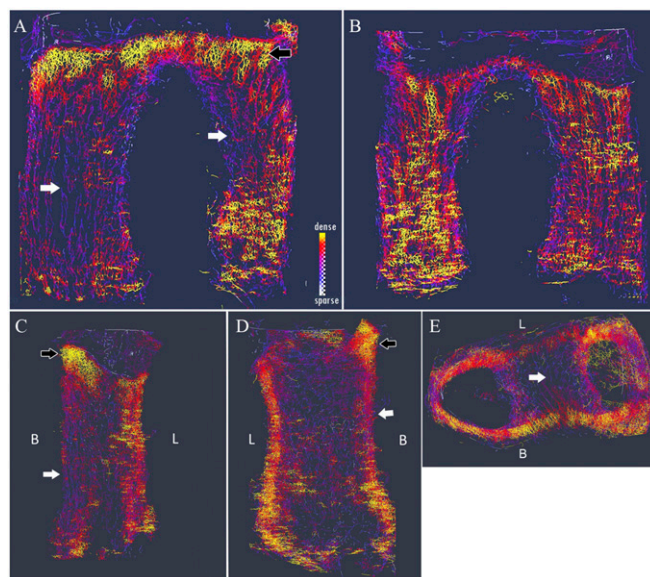


**Fig. 2.** Relative distribution maps of the PDL collagen network of a 15-wk-old mouse, hot colors toward yellow are high-density fibers; cooler colors toward blue are low-density fibers (sparse networks). *B*, buccal on cheek side; *L*, lingual on tongue side. (*A*) Sagittal view at the fiber distribution map on buccal half. Note the nonuniform fiber distribution and the dense collar at the uppermost region of the PDL tissue (black arrow); areas with sparser networks are shown with white arrows. (*B*) Sagittal view of the fiber distribution map of lingual half; fibers are distributed more evenly compared with the buccal side. (*C* and *D*) Coronal views showing the mesial root, located closer to the front of the mouth (*C*) and distal root, located closer to the back of the mouth (*D*). Note the differences in the densities between the lingual side (*L*) and the buccal side (*B*). A dense collar is located on the top of the buccal side (black arrow) and the sparse area in the middle of the root (white arrow). (*E*) Top view showing the sparse network in between the two roots, at the furcation region (white arrow).

of both roots contains only sparse networks (Fig. 2*A*, white arrows). This difference can be readily seen in coronal views of the roots (Fig. 2*C* and *D*). A greater difference in the distribution at the lingual and buccal sides is seen in the mesial root (Fig. 2*C*). Only sparsely distributed fibrous sheets are seen in the furcation area, between the roots (Fig. 2*E*, white arrow).

**Correlating Function with Fiber Distribution.** The loading system in the microCT enables vertical loading of the tooth similar to a physiological mastication process while it is still inside the bone (Fig. 3*A*) (13). The nonfixed, fresh conditions of the specimen allowed analysis of the tooth trajectory under functional loads. The morphology of molar teeth of many mammalian species, including humans and mice, is such that the long axis of the crown is not continuous with the long axis of the roots. An angle of  $\sim 25^\circ$  toward the buccal side exists between the two axes in the mouse molar (Fig. 3*B*), similar to the angle in a rat specimen (15). The loading system is designed such that the long axis of the crown will be continuous with the moveable anvil and perpendicular to the occlusal surface of the crown, similar to the direction of functional vertical loads. Here, the 3D scan in the compressed mode showed that the PDL space was getting narrow at the middle portions of the buccal surfaces of the roots as well as at the furcation (Fig. 3*C* and *F*), similar to what was shown in a rat model (15). The areas in the PDL that showed prominent narrowing and contact areas between the root and the bone were colocalized with areas in the PDL containing only few collagen sheets—the sparse networks (Fig. 3*C–F*, black arrows).

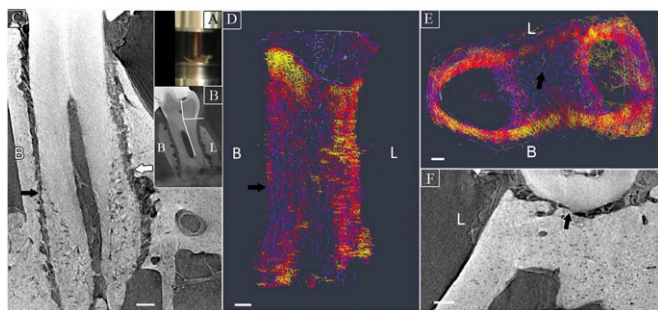


**Fig. 3.** Correlation between the fiber distribution and compression loads exerted on the PDL. (A) Closeup at the half mandible inside the loading setup with the vertically moving anvil bonded to the first molar. (B) A 2D slice from a microCT scan depicting the difference between the long axis of the crown and the long axis of the root. (C) Coronal 2D view of the mesial root imaged while the tooth was vertically compressed inside the loading setup showing a narrowing of the PDL region in the middle of the root at the buccal side (black arrow). Note the great proximity between the root and the bone. White arrow points at the widened area in the PDL. (F) Coronal 2D view in through the furcation when the tooth is vertically loaded, showing close proximity between the tooth and the bone at the furcation (black arrow). The density maps at an unloaded state (D and E) show that the regions of great proximity between the tooth and bone are occupied with sparse collagen networks (black arrows). B, buccal; L, lingual. (Scale bars: 100  $\mu\text{m}$ .)

**Structural Changes at Different Functional Stages.** To define whether tooth function is correlated with the distribution of dense and sparse fiber networks, we scanned specimens at different functional stages. We scanned teeth before eruption (2 wk after birth); right after eruption, when the teeth begin to function (3 wk); fully functioning in young adult mice (10 wk); and in adult mice (15 wk). Fig. 4 displays the density maps at the different stages. Interestingly, the same fiber distribution patterns are seen at all ages. The transverse sections (Fig. 4, *Right* column) show two features: (i) The furcation area, where the roots split, is generated as a sparse network before eruption, and remains as such during the different stages; and (ii) a dense fibrous strip (white arrows) surrounds the furcation area as well as the roots throughout all of the different functional stages, particularly in the prefunctional stage (2 wk). In the sagittal views (*Left* column), at the buccal side, sparse networks are seen in the middle of the roots (black arrowheads) and a dense network is encircling the *Upper* third. The lingual side is composed of both dense and sparse networks before eruption at 2 wk and gradually transforms into a uniform dense network as function is established. These features can also be seen in the coronal sections (*Middle* column). The fiber density at the mesial and distal surfaces of the roots is reduced once the tooth is starting to function.

To verify the different fiber densities detected by the microCT method, a second harmonic generation method was used. Fibrillar collagens generate a very bright second harmonic generation (SHG) signal (16). This signal is reflected intensely from noncentrosymmetric structures such as those of triple helical fibrous collagen molecules (17). We used the SHG signal from a PDL sample after the surrounding bone was reduced in its thickness to a transparency level that enabled the laser to penetrate through it. Fig. 5 is a composite showing the PDL–tooth–bone complex from the buccal side at the level where the roots emerge from the crown. According to the microCT scans this region contains the dense network strip. The SHG signal shows the same dense collagen network feature in this region (white arrows). The bone around the distal root was reduced such that exposure of the PDL along the root, where the sparse network is located, was revealed. Indeed, the SHG signal from the fibers in that area was weaker, corresponding to less organized and fewer

collagen networks (black arrow). Verification of the collagen type was done by immunostaining of collagen type I and imaging by SHG with two photon emission; both signals were overlapping (*SI Appendix*, Fig. S8).

**Directionality Analysis.** Visualizing the entire PDL fibrous component in 3D revealed that the longitudinal backbone of the fibers displays a certain directionality in the mesial–distal direction. We therefore carried out a 3D directionality analysis comparing the phi and theta angles for fully functioning PDL and preeruptive state PDL. For the analysis, we used the cylinder correlation and trace correlation line modules in Avizo software (Xfiber Extension version 9.4, Thermo Scientific; a detailed description can be found in *SI Appendix*). Briefly, the algorithm assigns a cylinder to each of the detected fibers in the 3D view according to a defined length, diameter, and curvature as specified by the user. Thereafter, analysis of the different cylinder parameters, such as angulation and length, are executed. Our analysis depicts the phi and theta angles as well as the correlation between theta angle values and fiber length. Fig. 6 *A–D* shows the results for the fully functioning PDL. The phi angles for the majority of the fibers in both the collar and root regions are below  $180^\circ$ ; this implies a preferred distal direction of fibers. More specifically, the phi angles of the collar region peak at  $30^\circ$ , whereas the angles in the root region peak at values around  $150^\circ$  (ignoring the  $180^\circ$  peak that is neutral in the sagittal plane). The theta angle analysis shows that the collar region in the fully functioning PDL is mainly containing obliquely to horizontally oriented fibers ( $80^\circ$  to the z axis), whereas a large portion of the fibers around the root but below the collar are vertically oriented at angles between  $10^\circ$  and  $30^\circ$  (Fig. 6 *B* and *D*). Correlating the fiber length with the theta angle shows that the vertical fibers are longer than the horizontal group. Looking at the PDL fiber direction analysis at preeruption stage—before function is gained (Fig. 6 *E–H*), it can be seen that there is a preferred orientation of the collagen network already at that stage. With respect to the collar region, the theta angle distribution is very similar to that of the adult mouse—with preferred distal orientation; however, the phi angles peak at  $130^\circ$  (ignoring the  $180^\circ$  peak). This is explained by the fact that the tooth representing the 2-wk-old mouse is from the contralateral side of the 15-wk-old mouse. Along the root there was no directional preference (Fig. 6 *G* and

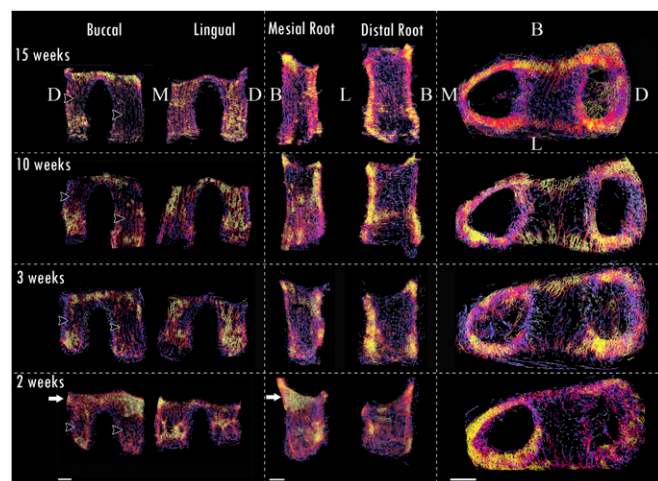


**Fig. 4.** Density map at different stages of development and function at 2 wk (before the tooth erupts), 3 wk (right after eruption), 10 wk (functioning tooth in young mouse), 15 wk (adult mouse). Density scale shows hot colors toward yellow (dense), cold colors toward blue (sparse). Black arrowheads point to sparse networks. (Scale bars: 200  $\mu\text{m}$ .)

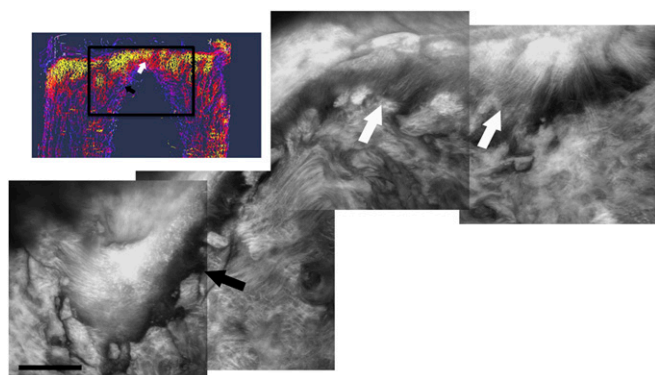


**Fig. 5.** Image of the stacked maximal projection of second harmonic generation signal from a 15-wk-old mouse. White arrows point to dense network, where the fibers are clearly observed, and black arrows point to the area occupied by a sparse network where fewer fibers are observed. Black rectangle in *Upper Left Inset* depicts the region imaged with the SHG signal. (Scale bar: 100  $\mu\text{m}$ .)

*H*). The longer fibers, however, were oriented vertically already in the prefunctional stage (Fig. 6*H*).

**Nonuniformity of the Noncollagenous ECM in the PDL.** The PDL is a highly vascularized tissue (18, 19). We demonstrate here that the sparse areas are correlated with high compression loads which in alveolar bone, unlike long bones, usually lead to bone resorption (20). However, under normal function and healthy conditions, the bone level in the furcation area is preserved despite the high

and repetitive compression forces. Therefore, we propose that bone remodeling rates are higher in the sparse than in the dense areas of the PDL. Previous studies showed high correlation between multipotent cells and blood vessels (18, 19, 21). Moreover, blood vessels serve as a conduit for bone marrow multipotent cells to get to the PDL and might play a central role in bone turnover. Fig. 7*A* shows a coronal section through the mesial root of a wild-type mouse stained with anti-CD31, an endothelial marker (green). Many blood vessels were seen at sparse networks, for example in the middle of the root on the buccal side (B) (white arrows), whereas only a few were seen on the lingual side (L) (black arrows) occupied by a dense network. To image blood vessels in different fiber network areas, we also used endothelial-specific *Flk1-Cre*; tdTomato transgenic mice (22). A sagittal section of the first molar shows large blood vessels at the furcation area (Fig. 7*B*, white arrows), but such vessels are absent from other areas in the PDL. To image the 3D distribution of blood vessels, we used multiphoton microscopy to image the PDL of *Flk1-cre*; tdTomato mice. Few small blood vessels were noted in the dense collar region while large vessels were located in the sparse network close to the furcation area (*SI Appendix*, Fig. S9). Epithelial rests of Malassez cells are residual cells from Hertwig's epithelial root sheath which is believed to have a central role in root formation (23). We noticed an extremely high presence of epithelial rests of Malassez cells in the furcation area (*SI Appendix*, Fig. S10). To further understand the contribution of different matrix components to the nonuniformity of the PDL, we examined the presence of chondroitin sulfate, decorin, and fibronectin in the different networks. Using immunohistochemistry we were able to detect noticeable differences in chondroitin sulfate levels between the networks. Higher levels of chondroitin sulfate

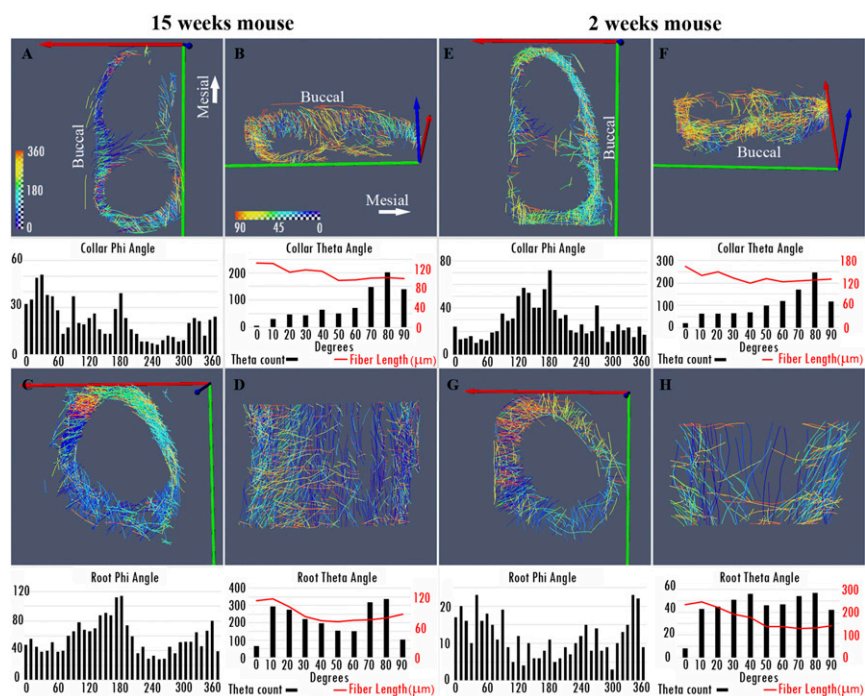


**Fig. 6.** Fiber directionality analysis displaying the phi and theta angles of a fully functioning tooth in a 15-wk-old mouse (A–D) and a nonfunctioning tooth, preeruption stage in a 2-wk-old mouse (E–H). The phi angle is an azimuthal angle in spherical coordinates and is measured in the xy plane from the x axis toward the y axis in a range of 0–360°. Theta angle is measured relative to the z axis in spherical coordinates. Due to the distinctly different characteristics of the collar region relative to the rest of the PDL fibers along the roots, we analyzed the direction of the collar region (A, B, E, and F) and the roots (C, D, G, and H) separately. When comparing the directionality of fibers between the roots, the distal root showed more uniformity in the fiber directionality; therefore, the results for the mesial root are displayed. To reduce processing time and increase the accuracy of the analysis, the root portion of the PDL was divided into three regions: upper, middle, and lower thirds. In general, areas closer to the collar region had a preferred direction compared with the apical thirds. Therefore, we show the results of the middle portion of the root as a representation for all three portions. x axis, red; y axis, green; z axis, blue. Phi angle analysis shows the counts in the y axis vs. measured angle in the x axis. The red line in the theta angle graph depicts the average fiber length in micrometers at each of the displayed angles.

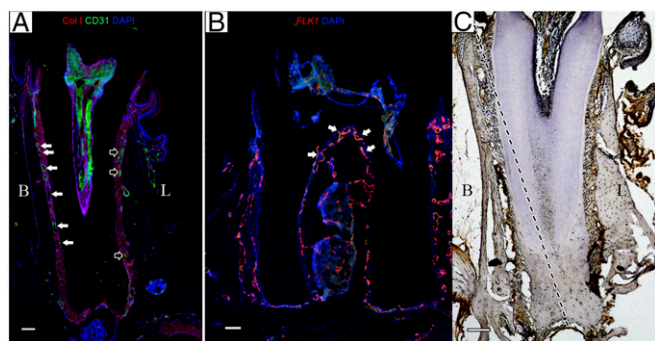


**Fig. 7.** Histological sections demonstrating the blood vessels inside the PDL. (A) A 2D coronal section of a 13-wk-old mouse; collagen fibers in the PDL are marked in red due to enhanced autofluorescence signal. White arrows point to the multiple blood vessels located in the buccal side, correlating with high compression forces area and the sparse collagen networks, as observed in Fig. 3. Black arrows show the few blood vessels found on the lingual side in regions of high density. (B) A 2D sagittal section. White arrows point to the large blood vessels observed at the furcation area in the PDL colocalized with low-density networks and high compression forces. (C) A 2D coronal section of a 12-wk-old *Flk1-cre*; *tdTomato* mouse through the mesial root, stained with antibody to chondroitin sulfate showing lower levels at the buccal side, B, compared with the lingual side, L. Higher levels are also found around blood vessels. Dashed line shows the sectioning direction of the sample in *SI Appendix*, Fig. S9. (Scale bars: 100  $\mu\text{m}$ .)

were correlated with dense networks as well as blood vessels (Fig. 7C), and, interestingly, it was very specific to cementocyte lacunae (*SI Appendix*, Fig. S10). Decorin and fibronectin levels were not associated with collagen density (*SI Appendix*, Fig. S11).

## Discussion

In this study, we show that the periodontal ligament is generated as a nonuniform entity. The distribution pattern of the different networks was shown to be preserved throughout different functional stages, and therefore the structure is preprogrammed to generate specific tooth function.

A very important area for tooth function is the furcation area between the roots of the tooth, acting as a fulcrum and exposed to compressive loads (15). Our results demonstrate that this area contains only a few collagen sheets, but numerous large blood vessels during different functional stages. A similar structure is found at injured sites in other ligament types. Ligaments are designed to work under tensional forces and contain mostly type I collagen (24); nonetheless, injuries to ligaments, typically caused by rupture, induce pathological changes that result in fewer type I collagen fibers with smaller diameters and increased vascularization (25, 26). Such regions are considered scars within ligaments; they function less efficiently in tension, but provide a better mechanism for enduring compressive forces (1, 24). The furcation area in the PDL sustains repeatedly high compression, torsion, and shear loads. Therefore, it can be regarded as a region of constant trauma, necessitating a structure that will reduce tissue damage. The presence of fewer type I collagen fibers and large blood vessels may leave more volume for noncollagenous ECM components. Such components, proteoglycans and GAGs, are found at sites exposed to compressive, torsional, and shear forces in other ligaments where they serve as load dissipaters and lubricators (27–29). However, when we examined the presence of noncollagenous ECM components, we found higher concentrations of chondroitin sulfate in the dense rather than the sparse networks, as well as with association to blood vessels. Noncollagenous ECM components are known to influence the stiffness of blood vessels either as structural components of the blood vessel wall (for example, elastin) or as an external component (28, 30–32). Therefore, due to the ligament preprogramming, blood vessels located in the

compression areas might have a different structure and mechanical properties to provide higher stability and resistance to ischemia incidents due to the repetitive compressive forces.

Local ischemia in the PDL is believed to occur due to compression forces and triggers orthodontic tooth movement (20, 33). However, the alveolar bone in the furcation area, constantly under compression forces, is not resorbed under normal conditions (34, 35). Previous studies showed that the contact areas between the tooth and the bone due to compression forces are small and localized (15, 36). As demonstrated here, the size of blood vessels in the compression regions are large and ischemia is therefore unlikely to readily occur there. Moreover, blood vessels serve as a conduit for pluripotent cells with the capacity to differentiate into bone-forming cells. The high presence of the rests of Malassez cells also provides further support for the high-differentiation capacity in the furcation region. We therefore suggest that the furcation area is specifically designed to function under compression loads. This could explain the enigmatic orthodontic observation that teeth with multiple roots move slower than single-rooted teeth at the same force levels. Initially orthodontic loads would trigger recruitment of multipotent cells and other mechanism to reinforce the resistance to compression loads rather than triggering bone resorption. Loads that exceed the dissipation capacity of the ligament may trigger different sensing units located outside of the PDL, such as osteocytes, and signaling pathways that eventually stimulate bone resorption and generate tooth movement (37).

Our results also show that the PDL fibrous network is divided into long vertical and short horizontal components. The longitudinal sheets can be regarded as the backbone of the fibrous component of the PDL. They are established before eruption and maintain their longitudinal orientation during the different functional stages. The horizontal element increases as function is gained, establishing the dense networks along the roots particularly on the lingual side. An exception to this pattern is the dense cervical collar region. This region, a unique structure surrounding the tooth just below the crown, contains a dense collagen network composed mostly of horizontal sheets. This structure exists before tooth eruption and is larger at the buccal side. Contrary to other dense regions, its dimensions are reduced after eruption. Since there is no pure horizontal movement of teeth, these dense horizontal fibers are likely to be under tension in all tooth movements and therefore possibly function as a main factor in guiding tooth movement. The reduction in its dimension with age may reflect changes that occur due to function and remodeling capacity. Our data also demonstrate that the fibrous PDL entity has a distal orientation even at preeruption stages and is prominently oriented to drive the tooth in a distal direction. This finding can possibly provide an explanation for the enigmatic physiological drift phenomenon of teeth. Teeth are showing constant drift throughout life in functioning teeth as well as when no functional forces exist. Human teeth have a mesial drift, whereas rodent teeth show a distal movement. Based on our findings, we suggest that the PDL has an internal force for tooth movement directed by the fibrous component, namely the horizontal group. This fact can open avenues for understanding tooth movement as well as bone formation and morphology.

Structural nonuniformities even at developmental stages are not unique to the PDL. The annulus fibrosus of the intervertebral disc, composed of type I collagen networks, was shown to sustain loads in a nonhomogenous pattern (38). Nonuniformities are detected already at the fetal stages; nevertheless, generally they are suggested to represent predisposition to future failure. Based on the data from this study, we suggest that nonuniformities are preprogrammed at developmental stages and are linked to normal ligament function. Support for this notion can be found in the literature, as nonuniformities were also seen in the 3D structure of the Achilles tendon (39) and at the fetal stage of the anterior cruciate ligament (40), suggesting that preprogramming for optimized function does occur.

## Conclusions

Here, we have used the periodontal ligament to show that non-uniformities in ligament structure occur before function. The non-uniformity is specifically designed to optimize the tissue function for future load regimes and it is not generated in response to pathological events. Areas that function under compression loads are generated with sparse collagen fibers and large blood vessels. Moreover, the fibers are organized in preferred orientations, providing internal forces that are optimal to particular function. We therefore propose that initially nonuniformities in ligaments are not structural modifications due to function, but are generated as a developmental structural strategy to optimize the tissue function.

## Materials and Methods

**Mice.** All animal experiments were performed in compliance with NIH's Guide for the Care and Use of Laboratory Animals and guidelines from the Harvard University Institutional Animal Care and Use Committee. The study was approved by the Harvard Medical School Institutional Animal Care and Use Committee (Protocol no. 02074).

Wild-type C57BL/6 mice were purchased from The Jackson Laboratory and served as controls.

*Flk1-Cre* mice (22) are a transgenic line generated by fusing the *Cre* gene to a fragment of the promoter sequence of *Flk1*. Reporter mice (tdTomato mice) were purchased from The Jackson Laboratory and crossed with the *Flk1Breier-Cre* to generate an endothelial cell-specific *Cre* strain inducing Tomato expression in endothelial cells only.

- Frank CB (2004) Ligament structure, physiology and function. *J Musculoskelet Neuronal Interact* 4:199–201.
- Amiel D, Frank C, Harwood F, Fronck J, Akeson W (1984) Tendons and ligaments: A morphological and biochemical comparison. *J Orthop Res* 1:257–265.
- Qu D, et al. (2017) Compositional mapping of the mature anterior cruciate ligament-to-bone insertion. *J Orthop Res* 35:2513–2523.
- Niyibizi C, Visconti CS, Kavalkovich K, Woo SLY (1995) Collagens in an adult bovine medial collateral ligament: Immunofluorescence localization by confocal microscopy reveals that type XIV collagen predominates at the ligament-bone junction. *Matrix Biol* 14:743–751.
- Niyibizi C, Sagarrigo Visconti C, Gibson G, Kavalkovich K (1996) Identification and immunolocalization of type X collagen at the ligament-bone interface. *Biochem Biophys Res Commun* 222:584–589.
- Benjamin M, Ralphs JR (1998) Fibrocartilage in tendons and ligaments—An adaptation to compressive load. *J Anat* 193:481–494.
- Vogel KG, Ordög A, Pogány G, Oláh J (1993) Proteoglycans in the compressed region of human tibialis posterior tendon and in ligaments. *J Orthop Res* 11:68–77.
- Petersen W, Tillmann B (1999) Structure and vascularization of the cruciate ligaments of the human knee joint. *Anat Embryol (Berl)* 200:325–334.
- Mandal BB, Grinberg A, Gil ES, Panilaitis B, Kaplan DL (2012) High-strength silk protein scaffolds for bone repair. *Proc Natl Acad Sci USA* 109:7699–7704.
- Matyas JR, Anton MG, Shrive NG, Frank CB (1995) Stress governs tissue phenotype at the femoral insertion of the rabbit MCL. *J Biomech* 28:147–157.
- Nanci A (2008) *Ten Cate's Oral Histology: Development, Structure, and Function* (Mosby, Elsevier, St. Louis), 7th Ed.
- Nanci A, Bosshardt DD (2006) Structure of periodontal tissues in health and disease. *Periodontol* 2000 40:11–28.
- Naveh GRS, Brumfeld V, Shahar R, Weiner S (2013) Tooth periodontal ligament: Direct 3D microCT visualization of the collagen network and how the network changes when the tooth is loaded. *J Struct Biol* 181:108–115.
- Naveh GR, Brumfeld V, Dean M, Shahar R, Weiner S (2014) Direct microCT imaging of non-mineralized connective tissues at high resolution. *Connect Tissue Res* 55:52–60.
- Naveh GRS, Shahar R, Brumfeld V, Weiner S (2012) Tooth movements are guided by specific contact areas between the tooth root and the jaw bone: A dynamic 3D microCT study of the rat molar. *J Struct Biol* 177:477–483.
- Williams RM, Zipfel WR, Webb WW (2005) Interpreting second-harmonic generation images of collagen I fibrils. *Biophys J* 88:1377–1386.
- Zipfel WR, et al. (2003) Live tissue intrinsic emission microscopy using multiphoton-excited native fluorescence and second harmonic generation. *Proc Natl Acad Sci USA* 100:7075–7080.
- Takimoto A, et al. (2015) Scleraxis and osterix antagonistically regulate tensile force-responsive remodeling of the periodontal ligament and alveolar bone. *Development* 142:787–796.
- Iwasaki K, et al. (2013) Periodontal ligament stem cells possess the characteristics of pericytes. *J Periodontol* 84:1425–1433.
- Meikle MC (2006) The tissue, cellular, and molecular regulation of orthodontic tooth movement: 100 years after Carl Sandstedt. *Eur J Orthod* 28:221–240.
- Chen SC, Marino V, Gronthos S, Bartold PM (2006) Location of putative stem cells in human periodontal ligament. *J Periodontol Res* 41:547–553.
- Licht AH, Raab S, Hofmann U, Breier G (2004) Endothelium-specific Cre recombinase activity in *flk-1-Cre* transgenic mice. *Dev Dyn* 229:312–318.
- Xiong J, Gronthos S, Bartold PM (2013) Role of the epithelial cell rests of Malassez in the development, maintenance and regeneration of periodontal ligament tissues. *Periodontol* 2000 63:217–233.
- Frank C, Amiel D, Woo SL, Akeson W (1985) Normal ligament properties and ligament healing. *Clin Orthop Relat Res*, 15–25.
- Peng B, Hou S, Wu W, Zhang C, Yang Y (2006) The pathogenesis and clinical significance of a high-intensity zone (HIZ) of lumbar intervertebral disc on MR imaging in the patient with discogenic low back pain. *Eur Spine J* 15:583–587.
- Yasuma T, Arai K, Yamauchi Y (1993) The histology of lumbar intervertebral disc herniation. The significance of small blood vessels in the extruded tissue. *Spine* 18:1761–1765.
- Smith SM, Shu C, Melrose J (2010) Comparative immunolocalisation of perlecan with collagen II and aggrecan in human foetal, newborn and adult ovine joint tissues demonstrates perlecan as an early developmental chondrogenic marker. *Histochem Cell Biol* 134:251–263.
- Vogel KG (2004) What happens when tendons bend and twist? Proteoglycans. *J Musculoskelet Neuronal Interact* 4:202–203.
- Melrose J, Smith SM, Appleyard RC, Little CB (2008) Aggrecan, versican and type VI collagen are components of annular lamellar crossbridges in the intervertebral disc. *Eur Spine J* 17:314–324.
- Davis GE, Senger DR (2005) Endothelial extracellular matrix: Biosynthesis, remodeling, and functions during vascular morphogenesis and neovessel stabilization. *Circ Res* 97:1093–1107.
- Califano JP, Reinhart-King CA (2010) Exogenous and endogenous force regulation of endothelial cell behavior. *J Biomech* 43:79–86.
- Wagenseil JE, Mecham RP (2009) Vascular extracellular matrix and arterial mechanics. *Physiol Rev* 89:957–989.
- Krishnan V, Davidovitch Z (2006) Cellular, molecular, and tissue-level reactions to orthodontic force. *Am J Orthod Dentofacial Orthop* 129:469.e1–469.e32.
- Nunn ME, Harrel SK (2001) The effect of occlusal discrepancies on periodontitis. I. Relationship of initial occlusal discrepancies to initial clinical parameters. *J Periodontol* 72:485–494.
- Pesun IJ (1997) Intrusion of teeth in the combination implant-to-natural-tooth fixed partial denture: A review of the theories. *J Prosthodont* 6:268–277.
- Naveh GRS, Weiner S (2015) Initial orthodontic tooth movement of a multirrooted tooth: A 3D study of a rat molar. *Orthod Craniofac Res* 18:134–142.
- Shoji-Matsunaga A, et al. (2017) Osteocyte regulation of orthodontic force-mediated tooth movement via RANKL expression. *Sci Rep* 7:8753.
- Han SK, et al. (2016) Optical coherence tomographic elastography reveals mesoscale shear strain inhomogeneities in the annulus fibrosus. *Spine* 41:E770–E777.
- Wu J-P, et al. (2017) High-resolution study of the 3D collagen fibrillary matrix of Achilles tendons without tissue labelling and dehydrating. *J Microsc* 266:273–287.
- Ferretti M, et al. (2007) The fetal anterior cruciate ligament: An anatomic and histologic study. *Arthroscopy* 23:278–283.